

Coupling effects and thin-shell corrections for surface instabilities of cylindrical fluid shells

Shuai Zhang ¹, Hao Liu ², Wei Kang ^{1,*}, Zuoli Xiao,^{1,3} Jianjun Tao,^{1,3} Ping Zhang,^{1,4} Weiyan Zhang,^{1,5} and X. T. He^{1,4}

¹HEDPS, Center for Applied Physics and Technology, and College of Engineering, Peking University, Beijing 100871, China

²Department of Applied Physics, School of Physics and Electronics, Hunan University, Changsha 410082, China

³Department of Mechanics and Engineering Science, College of Engineering, Peking University, Beijing 100871, China

⁴Institute of Applied Physics and Computational Mathematics, Beijing 100088, China

⁵China Academy of Engineering Physics, Mianyang 621900, China



(Received 26 August 2019; accepted 10 February 2020; published 25 February 2020)

We show that when linear azimuthal perturbations on the surfaces of a fluid shell are regrouped according to α^m , they can be divided into Bell model terms, coupling terms, and the newly identified thin-shell correction terms, where α is the ratio of R_{out} to R_{in} , and m is the mode number of a given unstable mode on the surfaces. It is also revealed that α^m is a convenient index variable of coupling effects, with which we show that the evolution of instability is composed of three stages, i.e., strongly coupled stage, transition stage, and uncoupled stage. Roughly, when $\alpha^m < 6$, the fluid shell is in the strongly coupled stage, where both coupling effects and the newly identified thin-shell corrections play important roles. Strong feed through is expected to be observed. The uncoupled stage is reached at $\alpha^m \sim 36$, where Bell's model of independent surface holds. In between is the transition stage, where mode competitions on the two surfaces are expected to be observed. These results afford an intuitive picture which is easy to use in guiding the design of experiments. They may also help to quickly grasp major features of instability experiments of this kind.

DOI: [10.1103/PhysRevE.101.023108](https://doi.org/10.1103/PhysRevE.101.023108)

I. INTRODUCTION

When a heavy fluid squeezes a light fluid, Rayleigh Taylor instability (RTI) [1,2] takes place at their interface. This phenomenon is also observed at the interfaces of multilayered targets of inertial confinement fusion (ICF) [3–6] and magnetoinertial fusion (MIF) [7–10] during the implosion process. It has been regarded as one of the most damaging factors that may seriously challenge the controllability of confinement fusion [4–6]. The instability not only destroys the geometrical symmetry of targets, but more seriously, it mixes hot fuel materials at the center with surrounding cold materials [5,6]. This may greatly reduce the burning efficiency of fuels and cause the failure of ignition [11]. Therefore, understanding the development of instability becomes an important issue of ICF and MIF.

In a simple planar configuration, the growth rate σ of an infinitesimal perturbation at the interface of two semi-infinite incompressible fluids is determined by $\sigma = \sqrt{A_t g k}$, where g is the acceleration, k is the wave number of the perturbation, and $A_t = 2|\Delta\rho|/\bar{\rho}$ is the Atwood number, with $|\Delta\rho|$ the density difference and $\bar{\rho}$ the average density of two fluids. Several improvements of this result, which include various effects, e.g., coupling effect [12], compressibility [13–15], rotation [16,17], and ablation [18–20], have been proposed in the past several decades. In a convergent geometry, however, the curvature and speed of the interfaces also contribute to σ , as was revealed by Bell and Plesset (BP) [21,22]. Recently, several groups further developed theories of the BP effect.

For example, Wang *et al.* [23] developed a weakly nonlinear model with the BP effect in cylindrical geometry, Epstein [24] considered the influence of uniform compression and geometrical convergence simultaneously, and Amendt *et al.* [25] considered the BP effect in their design of ICF target with a slightly modified BP model.

Surface instability of a fluid shell with finite thickness is more challenging. Interaction between the two surfaces contributes a further complexity in addition to the BP effect [23,26,27]. When the instability develops, the interaction between the two interfaces provides the possibility that perturbations on the unstable surface induce the development of ripples on the previously stable surface on the other side [28–30]. Several groups have tackled the problem. Mikaelian [31] derived a linear model to describe the BP effect and coupling between surfaces for a series of concentric cylindrical shells. Velikovich and Schmit [32] provided general linear perturbative solutions for spherical shells and solutions of helical and axial perturbations on cylindrical shells. In parallel with the development of theories, a number of experiments have been carried out to investigate instabilities with BP effect and coupling effect [33–37]. Special attentions have been paid to cylindrical geometry for its convenience to diagnostics.

Equipped with much improved experimental tools, there is a revived interest in the ICF community to reinvestigate the instability problem of a contracting fluid shell to reveal the details of how the instability grows. It is desirable that, in addition to mathematical formulas and curves, one can summarize some intuitive physical pictures or some rules of thumb for coupled fluid shells that are easy to use in guiding the design of targets or experiments. For this purpose, we propose to regroup linear perturbations on the surfaces of a

*weikang@pku.edu.cn

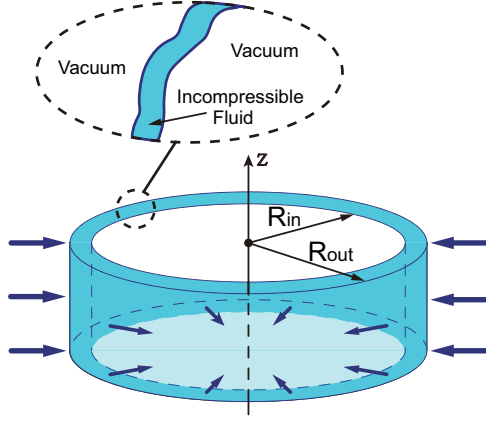


FIG. 1. Schematic illustration of a contracting cylindrical shell considered in this work. R_{in} and R_{out} here are inner and outer radii of undisturbed surfaces.

fluid shell with respect to α^m , where α is the ratio of R_{out} over R_{in} , and m is the mode number of a given unstable mode on the surfaces. The linear evolution equations can then be divided into Bell model terms, coupling terms, and the newly identified thin-shell correction terms according to the order of α^m . We find that by using α^m as a convenient index variable for coupling effects, the evolution of instability is composed of three stages, i.e., strongly coupled stage (roughly $\alpha^m < 6$), transition stage (approximately $6 < \alpha^m < 36$), and uncoupled stage (roughly $\alpha^m > 36$). At the strongly coupled stage, coupling effects and the newly identified thin-shell corrections play important roles, and strong feed through is expected to be observed at this stage. In the uncoupled stage, Bell's results [21] of two independent surfaces are recovered. Between these two is the transition stage, where mode competitions on the two surfaces are expected to be observed.

The rest of this article is organized as follows. In Sec. II, we show how to divide the linear evolution equations on the surfaces of a fluid shell into different groups according to the order of α^m , and how the coupling terms and thin-shell corrections are determined. In Sec. III, a systematic physical picture of coupling effects and thin-shell corrections is presented. Finally, we conclude our work with a short summary in Sec. IV with its potential application in experiments mentioned.

II. THEORETICAL MODEL AND FORMULAS

We consider a thin shell of cylindrical symmetry, i.e., without axial variations, which is a configuration convenient for experimental measurements [33,34], as schematically displayed in Fig. 1. The shell is composed of incompressible and inviscid fluid of density D . A cylindrical coordinate system attached to the center is used to describe the position of each point on both surfaces. Time dependent radii of undisturbed inner and outer surfaces are denoted as $R_{in}(t)$ and $R_{out}(t)$, respectively. During the contraction, the volume of the shell is viewed as a constant, which leads to the relation

$$\pi(R_{out})^2 = \pi(R_{in})^2 + \pi A, \quad (1)$$

with πA indicating the constant cross-section area of the shell. In term of the ratio

$$\alpha(t) \equiv R_{out}(t)/R_{in}(t), \quad (2)$$

one can write the velocity and the acceleration of inner surface as

$$\dot{R}_{in} = \frac{R_{out}\dot{R}_{out}}{\sqrt{(R_{out})^2 - A}} = \alpha\dot{R}_{out}, \quad (3a)$$

and

$$\ddot{R}_{in} = \alpha\ddot{R}_{out} - \alpha^3\frac{(\dot{R}_{out})^2}{R_{out}} + \alpha\frac{(\dot{R}_{out})^2}{R_{out}}, \quad (3b)$$

respectively, where the dots above letters represent time derivatives. From the definition of α in Eq. (2) and Eq. (3a), it is easy to get a symmetrical expression $R_{in}\dot{R}_{in} = R_{out}\dot{R}_{out}$.

If one further assumes that the contraction of the shell is irrotational, then the velocity of the fluid can be written as the gradient of a velocity potential Φ , which is the solution of the Laplace equation

$$\nabla^2\Phi = 0,$$

constrained by the two boundary conditions

$$D\left(\frac{\partial\Phi}{\partial t} + \frac{1}{2}(\nabla\Phi)^2\right) = 0 \quad (4)$$

and

$$\frac{\partial S(\rho, \theta, t)}{\partial t} + \nabla\Phi \cdot \nabla S(\rho, \theta, t) = 0, \quad (5)$$

at each surface. Here $S(\rho, \theta, t) = 0$ gives the time dependent motion of the surface in the cylindrical coordinates. ρ and θ are radial and azimuthal coordinates of a surface, respectively. Note that the perturbations along the axial (z) direction are not considered. For small perturbations η^{tot} on the cylindrical shell surfaces, it is convenient to express S as

$$S \equiv \rho - R(t) - \eta^{tot}(\theta, t). \quad (6)$$

The disturbed inner and outer surfaces of the shell are then $\rho = R_{in}(t) + \eta_{in}^{tot}(\theta, t)$ and $\rho = R_{out}(t) + \eta_{out}^{tot}(\theta, t)$, respectively.

We follow Bell's work [21] to consider a perturbation in the form of $\cos m\theta$. Here m is used to indicate the mode number of a certain perturbation. Only cosine part of the perturbation is used, as the sine part will provide similar result [21]. The total perturbation η^{tot} of both surfaces can then be written as power series of a formal parameter ϵ as

$$\eta_n^{tot} = \epsilon\eta_n \cos m\theta + O(\epsilon^2), \quad (7)$$

where the subscript n takes "in" or "out," representing the inner or outer surfaces. Note that ϵ in the expansion is only a formal parameter used to keep the order of perturbations. It will be set to be 1 later in numerical calculations.

A. Perturbative solutions to the first order

To the first order of ϵ , combining with $R_{in}\dot{R}_{in} = R_{out}\dot{R}_{out}$, velocity potential Φ is then derived from Laplace equation as

$$\Phi = R_{in}\dot{R}_{in} \ln \rho + \epsilon a(t)\rho^m \cos m\theta + \epsilon b(t)\rho^{-m} \cos m\theta, \quad (8)$$

where the time-dependent functions $a(t)$ and $b(t)$ can be solved with boundary conditions

$$\frac{\partial \Phi}{\partial \rho} = \dot{R}_{\text{in}} + \epsilon \dot{\eta}_{\text{in}} \cos m\theta + O(\epsilon^2), \quad (9)$$

at $\rho = R_{\text{in}} + \epsilon \eta_{\text{in}} \cos m\theta$, and

$$\frac{\partial \Phi}{\partial \rho} = \dot{R}_{\text{out}} + \epsilon \dot{\eta}_{\text{out}} \cos m\theta + O(\epsilon^2), \quad (10)$$

at $\rho = R_{\text{out}} + \epsilon \eta_{\text{out}} \cos m\theta$, which are obtained from linearization of Eq. (5). Substituting Eq. (8) into Eq. (4) on both surfaces, one obtains the governing equations for η_{in} and η_{out} as

$$\underbrace{\ddot{\eta}_{\text{in}} + 2 \frac{\dot{R}_{\text{in}}}{R_{\text{in}}} \dot{\eta}_{\text{in}} - (m-1) \frac{\ddot{R}_{\text{in}}}{R_{\text{in}}} \eta_{\text{in}}}_{\text{Bell model of inner surface}} - \underbrace{2m \frac{1}{\alpha^{2m}-1} \frac{\ddot{R}_{\text{in}}}{R_{\text{in}}} \eta_{\text{in}}}_{\text{Thin-shell correction}} = \underbrace{-2m \frac{\alpha^{m-1}}{\alpha^{2m}-1} \frac{\ddot{R}_{\text{in}}}{R_{\text{in}}} \eta_{\text{out}}}_{\text{Amplitude coupling term}} - \underbrace{-2m \frac{\alpha^{m-1}(-\alpha^2+1)}{\alpha^{2m}-1} \frac{\dot{R}_{\text{in}}}{R_{\text{in}}} \dot{\eta}_{\text{out}}}_{\text{Velocity coupling term}}. \quad (11)$$

$$\underbrace{\ddot{\eta}_{\text{out}} + 2 \frac{\dot{R}_{\text{out}}}{R_{\text{out}}} \dot{\eta}_{\text{out}} + (m+1) \frac{\ddot{R}_{\text{out}}}{R_{\text{out}}} \eta_{\text{out}}}_{\text{Bell model of outer surface}} + \underbrace{2m \frac{1}{\alpha^{2m}-1} \frac{\ddot{R}_{\text{out}}}{R_{\text{out}}} \eta_{\text{out}}}_{\text{Thin-shell correction}} = \underbrace{+2m \frac{\alpha^{m+1}}{\alpha^{2m}-1} \frac{\ddot{R}_{\text{out}}}{R_{\text{out}}} \eta_{\text{in}}}_{\text{Amplitude coupling term}} - \underbrace{-2m \frac{\alpha^{m-1}(-\alpha^2+1)}{\alpha^{2m}-1} \frac{\dot{R}_{\text{out}}}{R_{\text{out}}} \dot{\eta}_{\text{in}}}_{\text{Velocity coupling term}}. \quad (12)$$

Note that Eqs. (11) and (12) can also be expressed in different, but mathematically equivalent, forms, e.g., Eq. (10) of Ref. [31]. These various forms represent different motivations to tackle the problem. In this work, we regroup all terms with respect to the order of α , and divide them into three groups according to their effects as ‘‘Bell model,’’ ‘‘coupling terms,’’ and ‘‘thin-shell correction.’’ The coupling terms on the right-hand side of Eqs. (11) and (12) are roughly on the order of α^{-m} for large α , i.e., for a thick fluid shell. They can be further divided into ‘‘amplitude coupling’’ terms (ACT) and ‘‘velocity coupling’’ terms (VCT) according to their different origins. The thin-shell correction (TSC) terms get their names from the factor $1/(\alpha^{2m}-1)$. When the thickness of the shell decreases and α approaches 1, these terms become important. They also help to maintain the symmetry $m \rightarrow -m$.

When $R_{\text{out}}(t)$ or $R_{\text{in}}(t)$ is explicitly specified, η_{in} and η_{out} can then be obtained from Eqs. (11) and (12). Since $\alpha \equiv R_{\text{out}}/R_{\text{in}}$ is always greater than 1, it is not surprising to see that the coupling terms and thin-shell corrections can be dropped out when m or α is large. Keeping the leading terms, the two equations can be simplified to be

$$\ddot{\eta}_{\text{in}} + 2 \frac{\dot{R}_{\text{in}}}{R_{\text{in}}} \dot{\eta}_{\text{in}} - (|m| - 1) \frac{\ddot{R}_{\text{in}}}{R_{\text{in}}} \eta_{\text{in}} = 0, \quad (13)$$

and

$$\ddot{\eta}_{\text{out}} + 2 \frac{\dot{R}_{\text{out}}}{R_{\text{out}}} \dot{\eta}_{\text{out}} + (|m| + 1) \frac{\ddot{R}_{\text{out}}}{R_{\text{out}}} \eta_{\text{out}} = 0, \quad (14)$$

which recovers Bell’s result [21] on a single cylindrical interface and shows the decoupling of the two surfaces. However, as we shall show in the following discussions, the thin-shell correction and coupling terms in Eqs. (11) and (12) play dominant roles to small m mode perturbations of a thin shell, and thus cannot be neglected to get a correct physical picture.

B. Linear instability of two coupled surfaces

For a single surface, the instantaneous growth rate σ of an unstable mode would be enough to describe the linear instability of the surface. However, for a fluid shell, its two surfaces may be closely coupled, which makes it questionable to treat each surface independently while treat the coupling effects as a small perturbation to the surfaces. To get a systematic description of the coupled surfaces, we describe the perturbations on both surfaces with a two-component state vector $\Psi \equiv [\eta_{\text{in}}, \eta_{\text{out}}]^T$. The linearized governing equations Eqs. (11) and (12) can then be represented as

$$d^2 \Psi(t)/dt^2 = \hat{H}(t)d\Psi(t)/dt + \hat{G}(t)\Psi(t), \quad (15)$$

and the 2×2 matrices \hat{H} and \hat{G} are

$$\hat{H}(t) \equiv \begin{bmatrix} -2 \frac{\dot{R}_{\text{in}}}{R_{\text{in}}}, & -2m \frac{\alpha^{m-1}(-\alpha^2+1)}{\alpha^{2m}-1} \frac{\dot{R}_{\text{in}}}{R_{\text{in}}} \\ -2m \frac{\alpha^{m-1}(-\alpha^2+1)}{\alpha^{2m}-1} \frac{\dot{R}_{\text{out}}}{R_{\text{out}}}, & -2 \frac{\dot{R}_{\text{out}}}{R_{\text{out}}} \end{bmatrix},$$

and

$$\hat{G}(t) \equiv \begin{bmatrix} (m-1 + 2m \frac{1}{\alpha^{2m}-1}) \frac{\ddot{R}_{\text{in}}}{R_{\text{in}}}, & -2m \frac{\alpha^{m-1}}{\alpha^{2m}-1} \frac{\ddot{R}_{\text{in}}}{R_{\text{in}}} \\ 2m \frac{\alpha^{m+1}}{\alpha^{2m}-1} \frac{\ddot{R}_{\text{out}}}{R_{\text{out}}}, & -(m+1 + 2m \frac{1}{\alpha^{2m}-1}) \frac{\ddot{R}_{\text{out}}}{R_{\text{out}}} \end{bmatrix}.$$

Assuming Ψ approximately has the form of

$$\Psi(\delta t) \propto \exp[\xi \delta t] \begin{bmatrix} \omega \\ \beta \end{bmatrix}, \quad (16)$$

in a small time interval δt , one can derive a characteristic equation

$$(\xi^2 - \xi \hat{H} + \hat{G}) \begin{bmatrix} \omega \\ \beta \end{bmatrix} = 0 \quad (17)$$

from Eq. (15). Here, ω and β are components on the inner and outer surfaces, respectively. They are usually complex numbers, and $|\omega|^2 + |\beta|^2 = 1$. In general, there are four solutions for ξ , denoted as ξ_i , $i = 1, \dots, 4$, and each of ξ_i has

an eigen-vector $[\omega_i, \beta_i]^T$. The real part of each ξ_i is the instantaneous growth rate σ_i . Note that assuming Ψ having the form of Eq. (16) implies the motion parameters (e.g., \dot{R}_n, \ddot{R}_n , etc.) of the unperturbed shell vary much slower than those of perturbations, which we find applies to typical experimental conditions [32].

One can define instantaneous coupling factor

$$\Omega_i \equiv 2(|\omega_i|/|\beta_i|)/(1 + |\omega_i|^2/|\beta_i|^2), \quad (18)$$

which describes relative growth speed of perturbations on outer and inner surfaces for a certain unstable mode associated with ξ_i , as explained in Ref. [38]. According to the definition, Ω_i varies in the interval from 0 to 1. The two surfaces are independent when Ω approaches 0. While $\Omega = 1$ the two surfaces are strongly coupled.

In general, the coupling effect of an unstable mode depends on the growth rate σ_i and the coupling factor Ω_i . In a planar configuration, the two surfaces of a fluid layer in a vacuum environment only have one unstable mode with $\sigma = \sqrt{k g}$ and $\Omega = 2 \exp(k \Delta)/[1 + \exp(2k \Delta)]$, where Δ is the thickness of the fluid layer and k is the wave number [2,39]. Since σ here is independent of the thickness, the coupling effect of a fluid layer therefore only depends on the coupling factor Ω . This particular physical picture was further used to understand the coupling effect of a cylindrical shell of finite thickness [2,28,39]. However, it may seriously underestimate the complexity brought about by the σ . As we shall show in the following sections, the magnitudes of σ_i and Ω_i in a cylindrical configuration vary with the contraction of the shell, which leads to a major modification of the physical picture.

III. NUMERICAL RESULTS AND DISCUSSIONS

It is possible to get expressions of η_n from Eqs. (11) and (12) as function series of t , $R_{\text{out}}(t)$, $R_{\text{in}}(t)$ and their time derivatives, although it might be tediously long. Furthermore, with the lengthy expressions, one might lose the major physical picture, which is of great interest in implosion experiments and ICF target designs. We thus use numerical solutions to display important features of perturbation growth on both surfaces of a contracting cylindrical shell. In particular, we pay particular attention to the coupling effects between the two surfaces and finite thickness corrections.

To clearly display the influence of coupling effects and thin-shell corrections in different phases of contraction, two representative trajectories of $R_{\text{out}}(t)$, i.e.,

$$R_{\text{out}}(t) = \left[1 - \left(\frac{t}{t_{\text{max}}} \right)^2 \right] R_{\text{out}}(0), \quad (19)$$

and

$$R_{\text{out}}(t) = \left[1 - \left(\frac{t}{t_{\text{max}}} \right) \right] R_{\text{out}}(0), \quad (20)$$

are investigated in detail, where $0 \leq t < t_{\text{max}}$, and t_{max} is set to be 10 in later calculation. $R_{\text{in}}(t) \equiv \sqrt{[R_{\text{out}}(t)]^2 - A}$ is then also known and always greater than zero. The first trajectory represents an accelerated contraction, and the second one gives the feature of coasting contraction [40,41]. The degree of contraction is described by the convergence ratio $\text{Cr} \equiv$

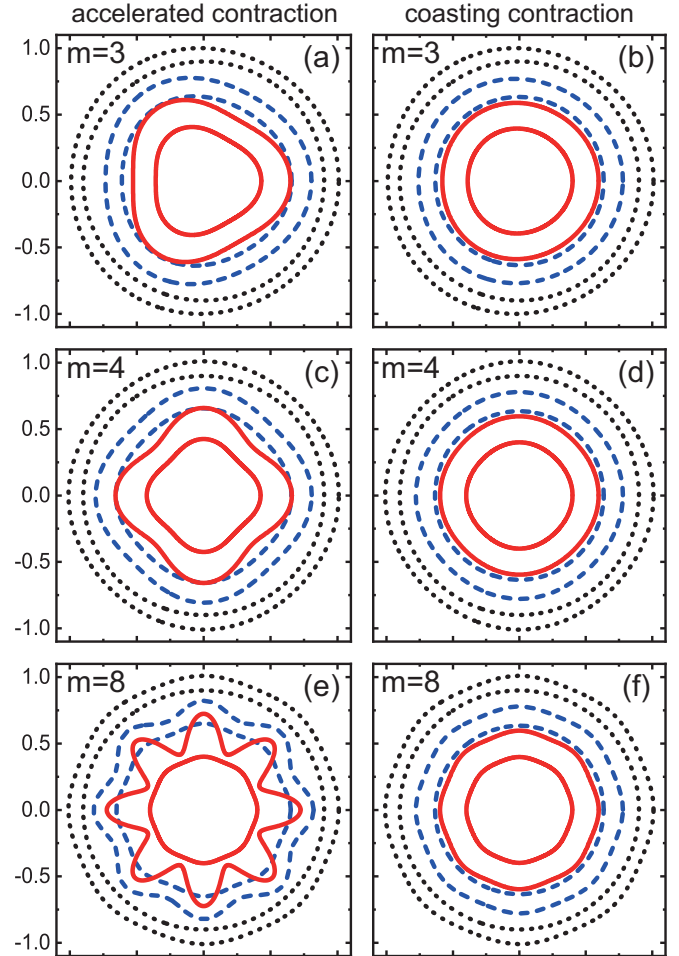


FIG. 2. Profiles of a fluid shell in accelerated (a, c, e) and coasting (b, d, f) contractions at $\text{Cr} = 1$ (black dots), 1.3 (blue dashed lines), and 1.7 (red solid lines), for mode number $m = 3$ (a, b), 4 (c, d), and 8 (e, f). The corresponding α are 1.11, 1.21, and 1.49. Their initial amplitude perturbations on outer surfaces have the same value $\eta_{\text{out}}(0) = 0.01$.

$R_{\text{out}}(0)/R_{\text{out}}(t)$ [42], which increases monotonically during the process.

Linear evolution of perturbations on a cylindrical shell are shown in Figs. 2 and 3 for mode number $m = 3, 4$, and 8, which gives a general picture of instability development. Perturbation growth in the accelerated contraction specified by Eq. (19) is displayed in the left column of each figure, and the growth along coasting trajectory Eq. (20) is presented in the right column for a close comparison. The initial aspect ratio of the shell [39] $R_{\text{out}}(0)/[R_{\text{out}}(0) - R_{\text{in}}(0)]$ is set to be 10, which is close to the ratio used in the experiments [43,44] and in ICF fuel capsules [39].

Initial perturbations are introduced in two ways following typical experimental setups [34,45] to highlight coupling effects between the two surfaces. One is ripples on the outer shell surface, i.e., amplitude perturbation $\eta_{\text{out}}(0)$ on the outer surface. Evolution of the perturbation is displayed in Fig. 2. The other is the perturbation of initial velocity on the outer surface, i.e., the velocity perturbation $\dot{\eta}_{\text{out}}(0)$ which is associated to pressure fluctuations or laser induced

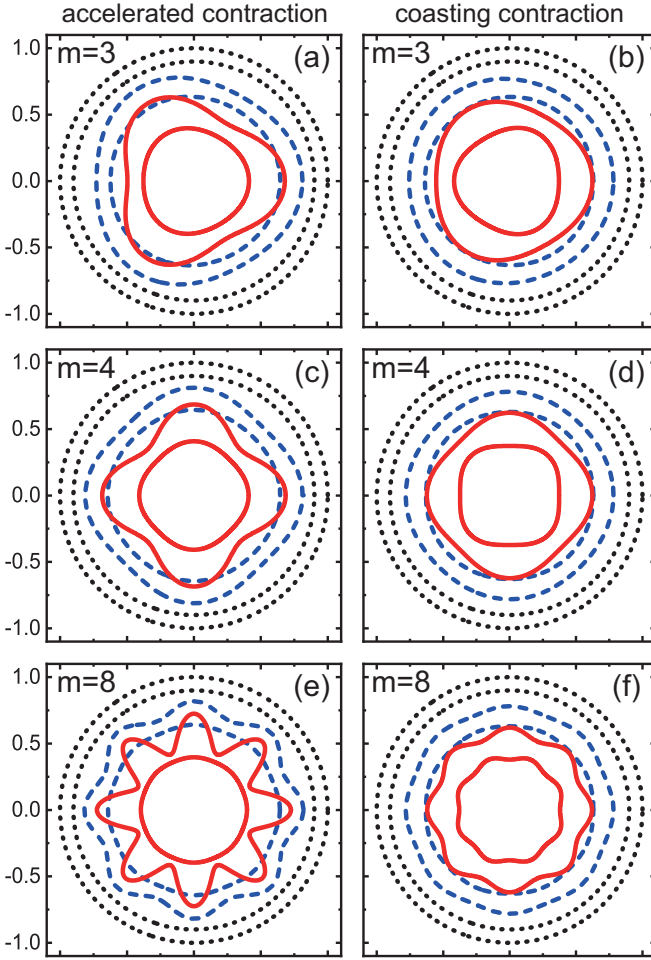


FIG. 3. Profiles of a fluid shell in accelerated (a, c, e) and coasting (b, d, f) collapse at $Cr = 1$ (black dots), 1.3 (blue dashed lines), and 1.7 (red solid lines), for mode number $m = 3$ (a, b), 4 (c, d), and 8 (e, f). The corresponding α are 1.11, 1.21, and 1.49. Their initial velocity perturbations on outer surfaces have the same value $\dot{\eta}_{\text{out}}(0) = 0.04\bar{v}$.

imprintings [46–48]. Figure 3 displays the development of velocity perturbations. The unit of $\eta_{\text{out}}(0)$ is $R_{\text{out}}(0)$, while the unit of $\dot{\eta}_{\text{out}}(0)$ is $\bar{v} \equiv R_{\text{out}}(0)/t_{\text{max}}$ for the convenience of further discussions. In both figures, the surfaces at $Cr = 1$, 1.3, and 1.7 (corresponding to $\alpha = 1.11$, 1.21, and 1.49) are drawn with different lines to show the evolution of instability.

Qualitatively, there are two features that can be immediately recognized from the figures. First, compared to the coasting contraction, the amplitude of perturbations on the outer surface is larger in accelerated contraction at the same convergence ratio Cr (and therefore the same α). This is a typical feature of RT instability, where the growth speed of a surface deformation increases with the surface acceleration and mode number m . Second, with the increasing of mode number m , the inner surface becomes less deformed, which suggests that coupling effects are more important at small m . This is in line with the fact that the coupling terms in Eqs. (11) and (12) are roughly proportional to α^{-m} . With the increasing of m , the coupling term becomes less important at the same α .

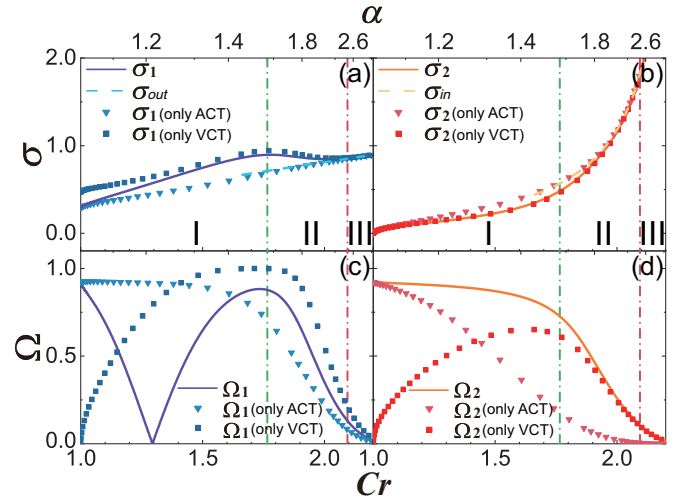


FIG. 4. Instantaneous growth rates σ_1 (a), σ_2 (b) and the instantaneous coupling factors Ω_1 (c), Ω_2 (d) for unstable mode $m = 4$ in an accelerated contraction. The green vertical dashed dots represent $\alpha^m = 6$, and the pink vertical dashed dots represent $\alpha^m = 36$.

A. Coupling effects

Figures 4(a) and 4(b) display the growth rates of a fluid shell as a function of Cr up to 2.2 [corresponding to $R_{\text{in}}(t) \approx 0.13$ and $\alpha \approx 3.53$] in an accelerated contraction, where σ_1 and σ_2 are the growth rates of the two most unstable modes, denoted by blue and red lines, respectively. Note that for a shell system, the third mode is a complex-conjugated mode of the second one. It shares the same σ and Ω as those of the second mode. The fourth mode is stable. It damps out quickly in the evolution. For illustrating purposes, an intermediate mode number $m = 4$ is chosen here. Note that σ_1 is not always the maximum growth rate. In fact, it is overtaken by σ_2 at the transition stage of contraction. The contribution of ACT to the growth rates, i.e., the growth rates calculated without VCT, are plotted as down-triangles in the figures, while those of VCT are plotted as square-dots. The growth rates

$$\sigma_{\text{in}} = \Re \left(\sqrt{\frac{(|m| - 1)\ddot{R}_{\text{in}}}{R_{\text{in}}} + \left(\frac{\dot{R}_{\text{in}}}{R_{\text{in}}}\right)^2} - \frac{\dot{R}_{\text{out}}}{R_{\text{out}}} \right), \quad (21)$$

and

$$\sigma_{\text{out}} = \Re \left(\sqrt{-\frac{(|m| + 1)\ddot{R}_{\text{out}}}{R_{\text{out}}} + \left(\frac{\dot{R}_{\text{out}}}{R_{\text{out}}}\right)^2} - \frac{\dot{R}_{\text{out}}}{R_{\text{out}}} \right), \quad (22)$$

solved from Eqs. (13) and (14) are also presented in dash-lines for large Cr as references of uncoupled limit of the two surfaces. Coupling factors for the first and second unstable modes are displayed in Figs. 4(c) and 4(d). Contributions of ACT and VCT are also presented in the same figures.

As displayed in Fig. 4, the evolution of instability is decomposed into three stages, i.e., strongly coupled stage (Region I in the figure), transition stage (Region II), and decoupled stage (Region III). The two boundaries of the stages are displayed as green and pink vertical dashed-dots in the figure. It turns out α^m is a convenient index variable to distinguish these stages. When α^m approaches 1, the coupling

terms in Eqs. (11) and (12) diverge roughly according to $1/(\alpha - 1)$, suggesting a strong-coupling limit. When α^m goes to infinity, the coupling terms diminish roughly according to α^{-m} , which is the decoupled limit. More importantly, α^m gives roughly the same boundaries for all unstable modes of different m . This will be convenient for experiments and target designs. Numerically, the first boundary can be determined to be $\alpha^m \sim 6$, where the Ω of the last unstable mode starts to decrease from nearly 1 to 0. The second boundary is set to be $\alpha^m \sim 36$, where the Ω of the last unstable modes drops to ~ 0.1 .

In the strongly coupled stage, perturbations on the two surfaces evolve as an inseparable entirety. As displayed in Fig. 4, at the beginning of the contraction, $\sigma_1 > 0$ and $\sigma_2 \sim 0$. At the meantime, Ω_1 is close to 1. This suggests that the evolution of perturbations is dominated by the first unstable mode, and perturbations on both surfaces grow at a similar speed. It is also noticed that the coupling effect at the beginning of an accelerated contraction is dominated by the ACT. As can be seen from Figs. 4(a) and 4(c), the σ_1 and Ω_1 calculated with only ACT contributions (down-triangles in the figures) are coincident with those calculated with all coupling terms (solid lines). This is a special feature of accelerated contraction. At the beginning of an accelerated contraction, as specified in Eq. (19), \dot{R}_n vanishes, which leads to a VCT contribution close to zero.

As the contraction continues, the second mode becomes unstable with the increase of \dot{R}_n and \ddot{R}_n , as displayed in Fig. 4(b). The cylindrical shell now has two unstable modes. In both unstable modes, VCT eventually overtakes ACT as the leading contribution of the coupling effects, however, in a different way. In the first unstable mode, VCT and ACT bear different signs and cancel each other. Figure 4(a) shows that σ_1 calculated with all coupling terms (solid lines) lies in between those σ_1 's calculated with VCT and ACT, and eventually gets close to the σ_1 with VCT (square dots). Meanwhile, Ω_1 calculated with all coupling terms (solid lines) decreases with the increase of Ω_1 calculated with only VCT, as displayed in Fig. 4(c). At $Cr = 1.3$ ($\alpha = 1.21$), the two contributions entirely cancel each other, and the two surfaces are decoupled temporarily. After that the coupling between the two surfaces recovers with further increase of VCT contributions.

Unlike the first unstable mode, VCT and ACT of the second unstable mode are cooperative, i.e., they do not cancel to each other, in calculating σ_2 and Ω_2 . The VCT dominates the coupling effect shortly after the accelerated contraction start, as can be seen from Fig. 4(b), where σ_2 of full coupling effects (solid lines) is very close to that calculated with VCT. Also, since VCT and ACT are cooperative, the two surfaces remain strongly coupled, as Fig. 4(d) shows.

It deserves to mention that even in the strongly coupled stage, the evolution of perturbations on the two surfaces of the fluid shell is not always controlled by the most unstable mode. Other less unstable modes may also be important due to temporarily decoupling caused by cancellation between ACT and VCT. For example, around $Cr = 1.3$, where $\Omega_1 = 0$, the most unstable mode is still the one associated with σ_1 . However, it only has component on one of the surfaces. The other surface then evolves according to the second unstable mode, i.e., the one associated with σ_2 .

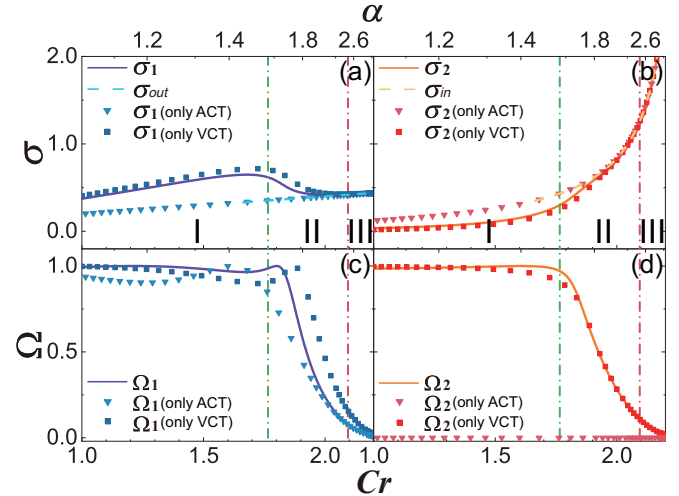


FIG. 5. Instantaneous growth rates σ_1 (a), σ_2 (b) and the instantaneous coupling factors Ω_1 (c), Ω_2 (d) for $m = 4$ in a coasting contraction. The green vertical dashed dot line represent $\alpha^m = 6$, and the pink vertical dashed dot line represent $\alpha^m = 36$.

In the transition stage, the coupling effect is dominated by VCT. The factor α^{-m} now gradually suppresses the coupling effect. This can be seen from Figs. 4(a) and 4(b) that, in Region II, the σ_1 and σ_2 gradually approach Bell's solution in Eqs. (21) and (22), which are displayed using dashed lines as the uncoupled limits of the growth rates. Also, coupling factors of both unstable modes start to drop to nearly zero in that region, as displayed in Figs. 4(c) and 4(d).

For cylindrical shells, another important feature of the transition stage is that the growth rate of the second mode overtakes that of the first mode, i.e., the second mode replaces the first one as the most unstable mode. Around the crossover, the growth of the perturbation on the surfaces of the shell is then determined by the competition of these two modes.

In the decoupled stage, the coupling effects are negligible. Figures 4(a) and 4(b) show that σ_1 is coincident with the growth rate σ_{out} of the outer surface, while σ_2 goes to the limit of σ_{in} . This means that the first unstable mode concentrates on the outer surface, while the second unstable mode is on the inner surface. The two surfaces are now completely isolated from each other and the Bell's results in Eqs. (21) and (22) are recovered.

Coupling effects in a coasting contraction is relatively straightforward, as we show in Fig. 5. For both unstable modes, VCT dominates the coupling effect from the very beginning. The brief decoupling of the first mode in the strongly coupled stage disappears, as displayed in Fig. 5(c). The instability at this stage is then only controlled by the unstable mode associated with σ_1 . The difference in Ω_1 between coasting and accelerated contractions can be traced back to the different behavior of \dot{R}_n . In the coasting contraction, $|\dot{R}_n|$ is always greater than zero, which leads to a finite contribution of VCT. In the accelerated contraction, $|\dot{R}_n|$ increases from zero, and VCT contribution is nearly zero at the beginning. This may afford a general picture of the coupling effect. Usually, VCT is the leading contribution to the coupling

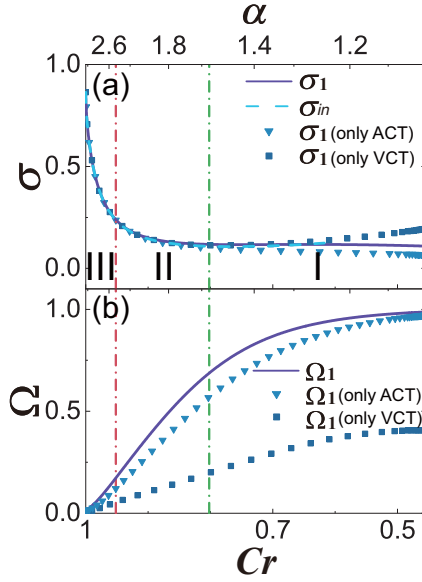


FIG. 6. Instantaneous growth rate σ_1 (a) and the instantaneous coupling factor Ω_1 (b) for mode $m = 4$ in an accelerated explosion. The green vertical dashed dot line represent $\alpha^m = 6$, and the pink vertical dashed dot line represent $\alpha^m = 36$.

effect, unless contracting speed of the surface is quite close to zero.

We would like to stress that, although these results are obtained with $m = 4$, the general picture holds for all mode numbers. It can be expected that the strongly coupled stage as well as the transition stage gets shorter, and the decoupled stage becomes longer when m increases. For example, for $m = 10$, as the experiment of Hsing *et al.* [33] focused on, the strongly coupled stage is relatively short. The shell enters the transition stage, around $Cr = 1.26$ ($\alpha = 1.20$), where the radius of the outer surface is about 80% of its original value. As a reference, the transition stage starts at $Cr \approx 1.76$ for $m = 4$. For small mode numbers like $m = 2$, most of the contraction takes place in the strongly coupled stage up to $Cr \approx 2.10$ ($\alpha \approx 2.49$).

For explosions, interactions between the two surfaces are slightly different. During the explosion, the thickness of the shell decreases monotonically, and there is only one unstable mode controlling the development of the instability, similar to the planar case [12]. Figure 6 displays the variation of the instantaneous growth rate σ_1 , and the coupling coefficient Ω_1 of the only unstable mode during the explosion. The trajectory of the outer surface is

$$R_{\text{out}}(t) = \left[1 + \left(\frac{t}{10} \right)^2 \right] R_{\text{out}}(0),$$

representing an accelerated explosion. The initial radii of both surfaces are $R_{\text{out}}(0) = 0.455$ and $R_{\text{in}}(0) = 0.129$, and the mode number m is 4. It shows that the Bell's result for the inner surface, denoted as σ_{in} , works well at early stages (the II and III stages in the figure) as expected. From the variation of Ω with respect to Cr , Fig. 6 also displays that the empirical criteria $\alpha^m = 6$ and 36 give good estimation to the boundaries dividing decoupled, transition, and strongly coupled stages.

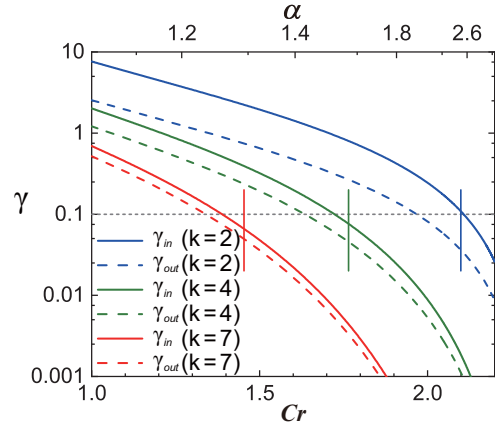


FIG. 7. Ratios γ_{in} and γ_{out} for $m = 2, 4$, and 7 , which represent the influence of thin-shell corrections. Short vertical segments shows the positions that $\alpha^m = 6$, at which γ drops to about 0.1.

B. Thin-shell corrections

Thin-shell correction terms are proportional to the RT terms, i.e., those terms associated with the acceleration of the surface in Eqs. (13) and (14). So, it is convenient to use the ratio γ of TSC over RT terms as a quantitative description of thin-shell effect. For the inner and outer surfaces, γ_{in} and γ_{out} is then defined as

$$\gamma_{\text{in}} \equiv \frac{-2m \frac{1}{\alpha^{2m-1}} \frac{\ddot{R}_{\text{in}}}{R_{\text{in}}} \eta_{\text{in}}}{-(m-1) \frac{\dot{R}_{\text{in}}}{R_{\text{in}}} \eta_{\text{in}}} = \frac{2m}{m-1} \frac{1}{\alpha^{2m-1}}, \quad (23)$$

and

$$\gamma_{\text{out}} \equiv \frac{2m \frac{1}{\alpha^{2m-1}} \frac{\ddot{R}_{\text{out}}}{R_{\text{out}}} \eta_{\text{out}}}{(m+1) \frac{\dot{R}_{\text{out}}}{R_{\text{out}}} \eta_{\text{out}}} = \frac{2m}{m+1} \frac{1}{\alpha^{2m-1}}, \quad (24)$$

respectively. Since γ_{in} and γ_{out} are only functions of m and α , which have nothing to do with the speed or acceleration of the surfaces, they can be used in both accelerated and coasting contractions and get the same conclusion. It is evident that the TSC are much larger than the original RT terms for a thin fluid shell because the factor $1/(\alpha^{2m-1})$ increases unbounded when α approaches 1 for a thin shell.

Figure 7 displays γ_{in} and γ_{out} as functions Cr for selected mode numbers $m = 2, 4$, and 7 , where solid lines represent γ_{in} , and dashed lines are for γ_{out} . Initially $R_{\text{out}}(0) = 1$ and $R_{\text{in}}(0) = 0.9$, the same as those used in the discussion of coupling effects. Vertical line segments are positions where $\alpha^m = 6$ for each mode number m . It shows that both γ_{in} and γ_{out} drop to about 0.1 at the places where $\alpha^m = 6$. That is to say, the time interval that TSC has a nonnegligible contribution is more or less coincident with the strongly coupled stage.

It is interesting to take a look of the thin shell limit of the instability, i.e., the limit of $\alpha \rightarrow 1$. With the notation $\zeta = \eta_{\text{in}} + \eta_{\text{out}}$ and $\delta = \eta_{\text{out}} - \eta_{\text{in}}$, the simplified equations with leading terms can be rewritten in a concise form as

$$\frac{\partial^2 \zeta}{\partial t^2} = -\frac{2\ddot{R}}{\varepsilon R} \delta, \quad (25)$$

and

$$\frac{\partial^2 \delta}{\partial t^2} + 4 \frac{\dot{\bar{R}}}{\bar{R}} \frac{\partial \delta}{\partial t} + 2 \left(\frac{\dot{\bar{R}}}{\bar{R}} \right)^2 \delta = -\varepsilon \frac{(m^2 - 1) \ddot{\bar{R}}}{2\bar{R}} \zeta, \quad (26)$$

with $\bar{R} = \sqrt{R_{\text{in}} R_{\text{out}}}$ and $\varepsilon = \alpha - 1$. They are similar to Mikaelian's results (Eqs. (20a) and (20b) of Ref. [31]), which were derived in a different way.

An analytical solution to Eqs. (25) and (26) would be difficult since $\ddot{\bar{R}}$ and $\dot{\bar{R}}$ are generally time-dependent. However, in two typical cases, one can get simple results. One is in the coasting contraction, where $\ddot{\bar{R}} = 0$. The most unstable perturbation on the surfaces grows proportional to $\exp[-(2 + \sqrt{2})(\dot{\bar{R}}/\bar{R})t]$. The other is at the beginning of an accelerated contraction, where $\dot{\bar{R}} = 0$ and the most unstable perturbation grows $\sim \exp[(m^2 - 1)^{1/4}(-\ddot{\bar{R}}/\bar{R})^{1/2}t]$.

IV. SUMMARY

In summary, we show that linear perturbations on the surfaces of a fluid shell can be divided into Bell model terms, coupling terms, and thin-shell correction terms, if the perturbations are regrouped according to α^m . It is also revealed that α^m is a convenient index variable for coupling effects, with

which we show the evolution of instability is composed of three stages as strongly coupled stage, transition stage, and uncoupled stage. Roughly when $\alpha^m < 6$, the fluid shell is in the strongly coupled stage, where coupling effects and thin-shell corrections play important roles. Strong feed-through effects are expected to be observed at this stage. The uncoupled stage is reached when approximately $\alpha^m > 36$, where Bell's picture of perturbations on two independent surfaces holds. Between these two is the transition stage, where one expects to see typical phenomena of mode competitions on the two surfaces. These results afford an intuitive picture which is easy to use in guiding the design of experiments. They also help to quickly grasp major features of instability experiments.

ACKNOWLEDGMENTS

This work is financially supported by the National Key Research and Development Program of China under Grant No. 2017YFA0403200, NSFC (Grant No. 11805061), Natural Science Foundation of Hunan Province, China (Grant No. 2019JJ50072), the Science Challenging Project under Grant No. TZ2016001, and the Fundamental Research Funds for the Central Universities.

-
- [1] L. Rayleigh, *Proc. London Math. Soc.* **s1-14**, 170 (1882).
 [2] G. Taylor, *Proc. R. Soc. London A* **201**, 192 (1950).
 [3] X. T. He, J. W. Li, Z. F. Fan, L. F. Wang, J. Liu, K. Lan, J. F. Wu, and W. H. Ye, *Phys. Plasmas* **23**, 082706 (2016).
 [4] S. E. Bodner, D. G. Colombant, J. H. Gardner, R. H. Lehmborg, S. P. Obenshain, L. Phillips, A. J. Schmitt, J. D. Sethian, R. L. McCrory, W. Seka, C. P. Verdon, J. P. Knauer, B. B. Afeyan, and H. T. Powell, *Phys. Plasmas* **5**, 1901 (1998).
 [5] H.-S. Park, O. A. Hurricane, D. A. Callahan, D. T. Casey, E. L. Dewald, T. R. Dittrich, T. Döppner, D. E. Hinkel, L. F. Berzak Hopkins, S. Le Pape, T. Ma, P. K. Patel, B. A. Remington, H. F. Robey, J. D. Salmonson, and J. L. Kline, *Phys. Rev. Lett.* **112**, 055001 (2014).
 [6] S. P. Regan, J. A. Delettrez, V. N. Goncharov, F. J. Marshall, J. M. Soures, V. A. Smalyuk, P. B. Radha, B. Yaakobi, R. Epstein, V. Y. Glebov, P. A. Jaanimagi, D. D. Meyerhofer, T. C. Sangster, W. Seka, S. Skupsky, C. Stoeckl, D. A. Haynes, J. A. Frenje, C. K. Li, R. D. Petrasso, and F. H. Séguin, *Phys. Rev. Lett.* **92**, 185002 (2004).
 [7] J. Ongena, R. Koch, R. Wolf, and H. Zohm, *Nature Phys.* **12**, 398 (2016).
 [8] C. Li and X. Yang, *Phys. Plasmas* **24**, 042705 (2017).
 [9] M. R. Gomez, S. A. Slutz, A. B. Sefkow, D. B. Sinars, K. D. Hahn, S. B. Hansen, E. C. Harding, P. F. Knapp, P. F. Schmit, C. A. Jennings, T. J. Awe, M. Geissel, D. C. Rovang, G. A. Chandler, G. W. Cooper, M. E. Cuneo, A. J. Harvey-Thompson, M. C. Herrmann, M. H. Hess, O. Johns, D. C. Lampa, M. R. Martin, R. D. McBride, K. J. Peterson, J. L. Porter, G. K. Robertson, G. A. Rochau, C. L. Ruiz, M. E. Savage, I. C. Smith, W. A. Stygar, and R. A. Vesey, *Phys. Rev. Lett.* **113**, 155003 (2014).
 [10] Y. Li, C. Zhai, G. Ren, J. Gu, W. Huo, X. Meng, W. Ye, K. Lan, and W. Zhang, *Matter Radiat. Extremes* **2**, 69 (2017).
 [11] J. Gu, Z. Dai, S. Zou, W. Ye, W. Zheng, P. Gu, and S. Zhu, *Matter Radiat. Extremes* **2**, 9 (2017).
 [12] K. O. Mikaelian, *Phys. Rev. A* **28**, 1637 (1983).
 [13] D. Livescu, *Phys. Fluids* **16**, 118 (2004).
 [14] H. Yu and D. Livescu, *Phys. Fluids* **20**, 104103 (2008).
 [15] I. B. Bernstein and D. L. Book, *Phys. Fluids* **26**, 453 (1983).
 [16] J. J. Tao, X. T. He, W. H. Ye, and F. H. Busse, *Phys. Rev. E* **87**, 013001 (2013).
 [17] B. B. Chakraborty, *Phys. Fluids* **25**, 743 (1982).
 [18] A. R. Piriz, *Phys. Plasmas* **8**, 997 (2001).
 [19] A. R. Piriz, J. Sanz, and L. Ibanez, *Phys. Plasmas* **4**, 1117 (1997).
 [20] T. Ikegawa and K. Nishihara, *Phys. Rev. Lett.* **89**, 115001 (2002).
 [21] G. I. Bell, Los Alamos National Laboratory, Los Alamos, NM, Report LA-1321 (1951).
 [22] M. S. Plesset, *J. Appl. Phys.* **25**, 96 (1954).
 [23] L. Wang, H. Guo, J. Wu, W. Ye, J. Liu, W. Zhang, and X. He, *Phys. Plasmas* **21**, 122710 (2014).
 [24] R. Epstein, *Phys. Plasmas* **11**, 5114 (2004).
 [25] P. Amendt, J. D. Colvin, J. D. Ramshaw, H. F. Robey, and O. L. Landen, *Phys. Plasmas* **10**, 820 (2003).
 [26] R. Adkins, E. M. Shelton, M.-C. Renoult, P. Carles, and C. Rosenblatt, *Phys. Rev. Fluids* **2**, 062001 (2017).
 [27] K. O. Mikaelian, *Phys. Rev. Lett.* **48**, 1365 (1982).
 [28] S. T. Weir, E. A. Chandler, and B. T. Goodwin, *Phys. Rev. Lett.* **80**, 3763 (1998).
 [29] K. Shigemori, H. Azechi, M. Nakai, T. Endo, T. Nagaya, and T. Yamanaka, *Phys. Rev. E* **65**, 045401(R) (2002).
 [30] Y. Y. Lau, J. C. Zier, I. M. Rittersdorf, M. R. Weis, and R. M. Gilgenbach, *Phys. Rev. E* **83**, 066405 (2011).
 [31] K. O. Mikaelian, *Phys. Fluids* **17**, 094105 (2005).

- [32] A. L. Velikovich and P. F. Schmit, *Phys. Plasmas* **22**, 122711 (2015).
- [33] W. W. Hsing and N. N. Hoffman, *Phys. Rev. Lett.* **78**, 3876 (1997).
- [34] W. W. Hsing, C. W. Barnes, J. B. Beck, N. M. Hoffman, D. Galmiche, A. Richard, J. Edwards, P. Graham, S. Rothman, and B. Thomas, *Phys. Plasmas* **4**, 1832 (1997).
- [35] D. L. Tubbs, C. W. Barnes, J. B. Beck, N. M. Hoffman, J. A. Oertel, R. G. Watt, T. Boehly, D. Bradley, P. Jaanimagi, and J. Knauer, *Phys. Plasmas* **6**, 2095 (1999).
- [36] Y. Li-Bing, L. Hai-Dong, S. Cheng-Wei, O. Kai, L. Jun, and H. Xian-Bin, *Chin. Phys.* **13**, 1747 (2004).
- [37] C. R. Weber, T. Döppner, D. T. Casey, T. L. Bunn, L. C. Carlson, R. J. Dylla-Spears, B. J. Koziolowski, A. G. MacPhee, A. Nikroo, H. F. Robey, J. D. Sater, and V. A. Smalyuk, *Phys. Rev. Lett.* **117**, 075002 (2016).
- [38] K. O. Mikaelian, *Phys. Fluids* **7**, 888 (1995).
- [39] S. Atzeni and J. Meyer-Ter-Vehn, *The Physics of Inertial Fusion: Beam Plasma Interaction, Hydrodynamics, Hot Dense Matter* (Clarendon Press, Oxford, UK, 2004).
- [40] D. L. Book and S. E. Bodner, *Phys. Fluids* **30**, 367 (1987).
- [41] K. S. Budil, B. Lasinski, M. J. Edwards, A. S. Wan, B. A. Remington, S. V. Weber, S. G. Glendinning, L. Suter, and P. E. Stry, *Phys. Plasmas* **8**, 2344 (2001).
- [42] J. P. Sauppe, B. M. Haines, S. Palaniyappan, P. A. Bradley, S. H. Batha, E. N. Loomis, and J. L. Kline, *Phys. Plasmas* **26**, 042701 (2019).
- [43] D. B. Sinars, S. A. Slutz, M. C. Herrmann, R. D. McBride, M. E. Cuneo, K. J. Peterson, R. A. Vesey, C. Nakhleh, B. E. Blue, K. Killebrew, D. Schroen, K. Tomlinson, A. D. Edens, M. R. Lopez, I. C. Smith, J. Shores, V. Bigman, G. R. Bennett, B. W. Atherton, M. Savage, W. A. Stygar, G. T. Leifeste, and J. L. Porter, *Phys. Rev. Lett.* **105**, 185001 (2010).
- [44] C. W. Barnes, S. H. Batha, A. M. Dunne, G. R. Magelssen, S. Rothman, R. D. Day, N. E. Elliott, D. A. Haynes, R. L. Holmes, J. M. Scott, D. L. Tubbs, D. L. Youngs, T. R. Boehly, and P. Jaanimagi, *Phys. Plasmas* **9**, 4431 (2002).
- [45] G. Malamud, M. Grosskopf, and R. Drake, *High Energy Density Phys.* **11**, 17 (2014).
- [46] R. P. Drake, *Astrophys. J.* **744**, 184 (2011).
- [47] R. Betti and J. Sanz, *Phys. Rev. Lett.* **97**, 205002 (2006).
- [48] Z. Li, Z. Wang, R. Xu, J. Yang, F. Ye, Y. Chu, Z. Xu, F. Chen, S. Meng, J. Qi, Q. Hu, Y. Qin, J. Ning, Z. Huang, L. Li, and S. Jiang, *Matter Radiat. Extremes* **4**, 046201 (2019).